Article

Photonic Sensor for Multiple Targets Detection under Adverse Weather Conditions in Autonomous Vehicles

Abhishek Sharma [1], Sushank Chaudhary [2,*], Jyoteesh Malhotra [3], Sunita Khichar [2] and Lunchakorn Wuttisittikulkij [2,*]

1 Department of Electronics Technology, Guru Nanak Dev University, Amritsar 143005, India
2 Department of Electrical Engineering, Wireless Communication Ecosystem Research Unit, Chulalongkorn University, Bangkok 10330, Thailand
3 Department of Engineering and Technology, Guru Nanak Dev University Regional Campus, Jalandhar 144007, India
* Correspondence: sushankchaudhary@gmail.com (S.C.); lunchakorn.w@chula.ac.th (L.W.)

Abstract: Detection and tracing of multiple targets in a real-time scenario, particularly in the urban setup under adverse atmospheric conditions, has become a major challenge for autonomous vehicles (AVs). Photonic radars have emerged as promising candidates for Avs to realize via the recognition of traffic patterns, navigation, lane detection, self-parking, etc. In this work we developed a direct detection-based, frequency-modulated photonic radar to detect multiple stationary targets using four different transmission channels multiplexed over a single free space channel via wavelength division multiplexing (WDM). Additionally, the performance of the proposed photonic radar was examined under the impact of adverse weather conditions, such as rain and fog. The reported results in terms of received power and signal-to-noise ratio (SNR) showed successful detection of all the targets with bandwidths of 1 GHz and 4 GHz. The proposed system was also tested for range resolution of targets at 150 m and 6.75 cm resolution with 4 GHz bandwidth was reported, while resolution of 50 cm was reported with 1 GHz of bandwidth.

Keywords: autonomous vehicles; fog; photonic radar; rain; wavelength division multiplexing

1. Introduction

The World Health Organization was alarmed by the number of deaths and fatal injuries due to speeding, intoxication, and negligence [1]. The U.S. Department of Transportation has reported that around 94% of accidents that occurred in the U.S. are due to human negligence [2]. Automation in transportation has some intriguing predictions, such as lane capacity improvement, reduction in fuel consumption, emissions reduction, reduced travel time, etc. [3]. Thus, autonomous vehicles (AVs) have gained much attention as a new transportation system in the last decade [4]. To achieve autonomy in vehicles, the fusion of many sensors is proposed and studied to observe the contiguous atmosphere, such as traditional radars [5,6], photonic radars [7–10], and cameras [11,12]. Among these, photonic radars have gained lots of attention due to its high resolution and long-range target detection with precise distance measurements [13]. Several advantages, such as multiple target detection, blind-spot monitoring, lane and crossroads detections, and parking assistance, to name a few, that enhance the driving assistance experience in day-to-day events [14]. In contrast with the traditional microwave radars that employs radio frequency which is affected by the electro-magnetic interference and results in poor resolution and low bandwidth [15], the photonic radar modulates radio-frequency signal with optical signal (laser/led) and transmits it using optical lens as the transmitter into the free space.

Traditionally, radars are configured as pulsed radar and continuous wave (CW) radar, and the range is measured calculating the time of flight. Photonic radars are generally based upon frequency modulated (FM) CW radar configuration where range is measured by the

frequency of echo signal and bandwidth of the operational frequency [16–18]. Further, triangular sweep is favored in high-speed target detection since it offers smaller sweep time than the pulsed sweep [19]. Similarly, linearly frequency-modulated (LFM) RF signal with a saw-tooth (triangular) modulation function is established to determine object range and velocity [20]. Traditional radars have poor resolution; hence, they cannot distinguish adjacent targets due to high beam divergence, while photonic radars offers low beam divergence due to narrow line-width and hence, offers high-range resolutions and can differentiate between two targets separated by a few centimeters [21].

The FM-modulated photonic radars are engaged in direct detection realization with the benefit of more sensitivity to the echoes on the outlay of shorter detection range [22,23]. Another noticeable solution is heterodyning mixing, more commonly known as coherent detection, with benefits of high receiver sensitivity, longer ranges, and minimal signal fading than direct detection at the cost of system complexity [24,25]. Furthermore, the input power requirement is another challenge in any detection system used in the autonomous vehicle industry as limited power can be availed from vehicle batteries [26]. Photonic radars are provided with power efficient means of detections, and the reported system has successfully operated with input power as low as −10 dBm.

With the existing infrastructure, the absorption peaks emerge at 24 GHz and 60 GHz, which are rather high, and conveniently, some transmission windows are accessible for acquiring the broadcast of the signal amid these peaks. However, with increasing frequency, the effects of atmospheric turbulences become more severe and thus, restrict radars operations. Thereby, placing a limitation in attaining extended target detection-oriented applications confines the operating frequency in smaller ranges. Moreover, the microwave band centered radar signal has the considerable consequence of rainfall attenuation due to scintillation, rainfall, scattering, foliage blockage, and diffraction. Generally, the wavelengths become smaller in mm-band; therefore, truncated resonances are acknowledged that cause weak signal response. The most prevalent atmospheric turbulences consist of fluctuations in the refractive index due to variations in temperature and pressure as well as smog or dust particles, fog, and rainfall [27]. Regardless of its initial stages, various significant efforts affirming AVs have been presented here. Self-driving vehicles under the effects of smoke and dust particles in the atmosphere are discussed [28]. Another study [29] discusses and compares the effects of 950 nm and 1550 nm on photonic radar operations and the effects of turbulences on them. The influence of different fog situations and experimental calculations of the photonic radar is premeditated [30]. The electro-optical photonic radar is tested with uneven perceptibility changes in haphazard atmospheric conditions by simulations [31]. A consequence of distinctive gases has been calculated to understand turbulences due to low ambient temperature upon photonic radars [32].

Therefore, the described work accords the influence of different attenuations due to atmospheric situations upon the working efficacy of the photonic radar, mainly at a high frequency. Nevertheless, a limited study has been reported that confirms the effectiveness of a frequency-modulated continuous wave (FMCW) driven photonic radar system while considering the fading effects of atmospheric turbulences, such as rain, haze, and fog.

Another challenge in realizing high resolution is bandwidth selection, as a higher bandwidth tends to provide higher resolution. To attain higher bandwidth and ultimately the precise resolution, millimeter band (30–300 GHz) is preferred in photonic radars for operating frequency [33]. Lidar functions in 24 GHz band are generally recognized as ISM (industrial, scientific, and medical) band with unrestricted narrow band (NB) bandwidth of 250 MHz (24–24.5 GHz) and comprises a bandwidth of 5 GHz termed as ultra-wide band (UWB). Although NB-ISM band is employed in sensing blind spots, UWB-ISM is employed for greater resolution. With new guidelines, UWB will not be available shortly, and hence, ISM band would not be as striking as of now for autonomous vehicle uses [33]. Originally, radar works in 70 GHz band, and 70–77 GHz is accessible for autonomous transportation applications. The 77–81 GHz (with 4 GHz bandwidth) band is recognized as short range radar (SRR) band. The key assistance offered is high tolerable equivalent isotopic radiated

power (EIRP) that allows adaptive cruise control [33]. The range resolution obtainable by 77 GHz with frequency by 4 GHz bandwidth is 4 cm, equated to a range resolution of 75 cm and presented at 24 GHz with the bandwidth of 250 MHz.

Further, to widen the available bandwidth and track more than one target, the use of the multiplexing technique is proposed. WDM- (wavelength division multiplexing) centered optical links are preferred over the orthodox signal dissemination structures due to their compact and light weight structure, low loss, and immunity to electro-magnetic interference (EMI) [34].

2. Related Works and Main Contributions

In 2016 [35], synthetic aperture radar was proposed by the authors, incorporating the multibeam technique and WDM scheme to achieve high resolutions. In 2017 [36], another photonic synthetic aperture radar was designed which attained the bandwidth of 600 MHz and Ku Band. In another work [37], authors proposed a photonics-based, dual-band linear frequency-modulated continuous wave (LFMCW) radar receiver which offered high bandwidth as well as high resolution. In another work [38], authors demonstrated the detection of a one-inch metallic cylinder at a distance of 150 m by incorporating photonic radar based on 90 GHz FMCW radar with radio over fiber technology. In 2018 [39], authors proposed photonic time-stretch coherent radar (PTS-CR) which offered range resolution of 1.48 cm. The authors used an erbium-doped fiber amplifier for improving the signal-to-noise ratio (SNR) and proposed that PTS-CR can be operated over W band with 12 GHz ultra-broad bandwidth. In 2020 [8], the authors proposed silicon-chip-based photonic radar for attaining high resolutions. The reported result showed the resolution of 2.7 cm with error of less than 2.75 mm. Moreover, the detection of multiple targets was also reported with the help of inverse synthetic aperture. In another work [40], the authors proposed photonic radar based on the FMCW technique which is able to detect a single target. The authors also evaluated the performance under different atmospheric conditions, particularly rain and fog. Recently in 2021 [20], microwave photonic radar was demonstrated to detect the distance and velocity of a target with maximum error of 2.6% and 0.21%, respectively. Furthermore, in the literature, many key works with the use of wavelength division multiplexing were reported [41–44]. A novel MIMO-based photonic radar was reported based on the WDM technique that employed a single photonic-based trans-receiver and demonstrated simulation results of 15 × 15 MIMO radar system [45]. Microwave photonic radar using WDM was reported with 7.3 cm of range resolution [46]. Another work reported the use of the WDM technique in photonic integrated circuit (PIC) for high speed, low cost, and 3D sensing lidar systems [47].

In this work, we propose a direct detection linear frequency modulated continuous wave (LFM-CW) based photonic radar by modulating a carrier frequency of 77 GHz with bandwidths of 1 GHz and 4 GHz to realize the autonomous vehicles. The system is designed to range and detect multiple targets, as shown in Figure 1. The free space link is modeled using MATLAB$^{\text{TM}}$, while the system is designed using OptiSystem$^{\text{TM}}$ software.
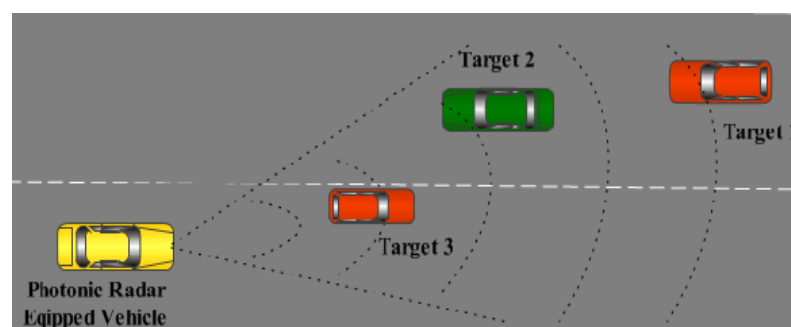

Figure 1. General diagram of tracking of multiple targets using photonic radars in autonomous vehicles [18].

The main contributions in this work are briefed as follows:

- Designing a small and economical photonic radar system;
- Testing the system under adverse weather conditions using four targets in a complex recognition scenario;
- Evaluating the impact of different bandwidths in detection as well as on range resolution of multiple targets.

The remaining paper is organized as Section 3 presents the system modeling and working principle of proposed system, Section 4 describes the interpretations and discussion of results, followed by Section 4 which presents the conclusion of this work.

3. System Modeling and Working Principle

Figure 2 depicts the schematic illustration of the proposed linear frequency modulated continuous wave (LFM-CW) wavelength division multiplexing (WDM) enabled photonic radar in direct detection configuration. The key advantage is low-power requirement and compact size that is a must for autonomous vehicles. At the transmitter side, the system contains four channels being transmitted using a single channel in free space over 150 m. Each channel comprises a saw tooth generator with a sample rate of 819.19 Mbps, and max amplitude of 1 a.u. is employed to generate triangular sweep signal, as discussed in the introduction. The input for this saw tooth generator is given by a pseudo random bit sequence generator, generating 90 kbps of signal. The triangular sweep signal is fed into linear frequency modulator (LFM) where information is modulated using center frequency of 77 GHz. As the system is tested for effects of bandwidth on resolution, the two bandwidths used are 1 GHz and 4 GHz. The range frequency peak, f_R, that denotes the target detection is calculated as Equation (1) [22]:

$$f_R = (2 \times R \times B)/(T_{(s)} \times C) \tag{1}$$

where R is the range in meters, aB is bandwidth, c is speed of light, and T_s is sweep time. A higher Q factor of linear frequency modulator is attained by equalizing the sweep rate of frequency and trip time of local oscillator [48]. The modulator transfer function is stated in Equation (2) as [49–51]:

$$\frac{E_{out}}{E_{in}} = \cos\left(\phi_o + \frac{\pi\,S(t)}{2v_\pi}\right) \tag{2}$$

where E_{out} and E_{in} are the input and output optical fields, v_π is the voltage needed to vary the optical power transfer function [50], ϕ_i is the initial phase, and $S(t)$ is the RF-LFM signal power that is defined as Equation (3):

$$S(t) = A_c \cos\left(2\pi f_c t + \frac{\pi B}{T_m}\,t^2\right) \tag{3}$$

where f_c is the center frequency, Ac is the amplitude of LFM signal, and B is the sweep bandwidth.

The output signal of this LFM modulator is split into two parts: one is fed into dual port Mach–Zhender modulator (DP-MZM) where the optical carrier is modulated with radio signal, and the other is mixed with the received signal to recover the detected signal. A continuous wave laser diode is used as the optical source, operating at 1550 nm for channel 1 and with 0.1 nm channel spacing for subsequent channels. The major contribution of this system is minimal power requirement as the laser operates at −10 dBm of input power, and the line width used is 100 KHz. The optical signal is fed into one port of lithium niobate (LiNbO$_3$) Mach–Zhender modulator and is used as the carrier signal. This LiNbO$_3$ modulator has an extinction ration of 30 dB, switching bias voltage of 4 V, switching RF voltage of 4 V, and bias voltages V1 and V2 as 0 V. External DC bias of 2 a.u. is applied to the

DP-MZM to generate second order sidebands and quash any additional sidebands if any. The DP-MZM output power for the direct detection systems is stated as Equation (4) [50]:

$$E_{Tx}(t) = \sqrt{\frac{P_t}{2}} \left[1 + \frac{\beta}{2} \cos\left(2\pi f_c t + \frac{\pi B}{T_m} t^2\right)\right] \cdot e^{(j\omega_o t + \theta_o(t))} \tag{4}$$

where β is the modulation index ($\beta << 1$); ω_o is the angular frequency of transmitted signal; and $\theta_o(t)$ is the random phase component.
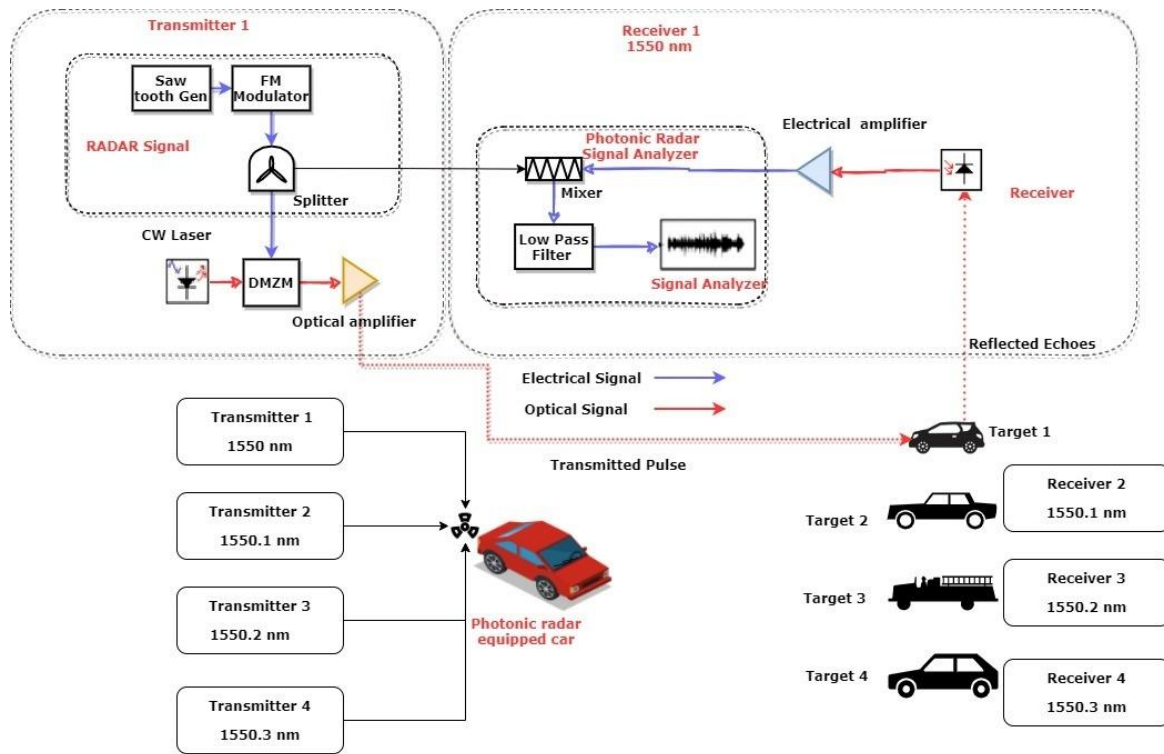

Figure 2. Schematic of proposed WDM-enabled LFMCW photonic radar. LFM: linear frequency modulator, DP-MZM: dual port Mach–Zehnder modulator, Tx/Rx: trans-receiver, EA: electrical amplifier, LPF: low-pass filter, WDM: wave-length division multiplexing.

To minimize the budget and size, the use of an optical amplifier is omitted in this proposed system. The optically modulated radar signal from each channel with different operating wavelengths is then fed into the wavelength division multiplexer (WDM) with a bandwidth of 10 GHz. The multiplexed signal is then focused on the target, transmitted over free space using the optical transmitter and receiver (telescopic lens) with apertures of 5 cm and 15 cm, respectively. The free space channel is simulated for a maximum target distance of 150 m with geometric losses, transmitter losses of 1 dB, and additional losses of 2 dB for compensating normal conditions. The reflected echoes from the target usually suffer losses, specifically from angular dispersion, atmospheric transmission effects, and target reflectivity. The reflected signal power at the receiver is calculated as in Equation (5) [22]:

$$P_r = \begin{cases} P_t \dfrac{\rho_t \ D^2 \ \tau_{opt} \tau_{atm}^2}{4R^2} & for\ extended\ target \\ P_t \dfrac{\rho_t \ A_t D^2 \ \tau_{opt} \tau_{atm}^2}{4R^2 A_{ill}} & for\ any\ target \end{cases} \tag{5}$$

where D is the receiver aperture diameter, ρ_t is the target reflectivity, A_t is the target area, τ_{opt} is the transmission loss in the optical domain, τ_{atm} is the atmospheric loss factor, A_{ill} is the illuminated area at target, and R is the target range.

The echoed signal power, E_{ref}, at receiver is given as in Equation (6) [22]:

$$E_{ref}(t) = \sqrt{P_r} \left[1 + \frac{\beta}{2} \cos(2\pi f_c (t - \tau) + \frac{\pi B}{T_m} (t - \tau)^2 \right] \cdot e^{(j(\omega_o - \omega_d)t + \theta_{o(t)})} \tag{6}$$

where τ is the propagation delay given as $\tau = 2 \times R/c$. With the range of 150 m, the delay time is computed as 1 µs.

The photodiode output current with the responsivity, $\Re$, is expressed as in Equation (7) [52]:

$$i_{ph}(t) = \Re.P_r \left(1 + \frac{\beta}{2} \cos(2\pi f_c (t - \tau) + \frac{\pi B}{T_m} (t - \tau)^2 \right)^2 \tag{7}$$

The filtered photocurrent signal to acquire the baseband signal is given as in Equation (8):

$$i_{ph}(t) = I_{dc} + i_{sig}(t) \approx \Re.P_r \left(1 + \frac{\beta}{2} \cos(2\pi f_c (t - \tau) + \frac{\pi B}{T_m} (t - \tau)^2 \right)^2 \tag{8}$$

where I_{dc} and i_{sig} are the dc and ac photo detected current signals.

The detector used is PIN type photodiode with responsivity of 1 *A/W* with dark current of 10 *nA*, load resistance of 50 Ω, and bandwidth (thermal as well as shot) of 410 MHz. An electrical analyzer is used to detect the power and signal-to-noise ratio of received signal as in Equation (9) [22]:

$$SNR_{dir} = \frac{\beta^2 \Re^2 P_r^2 / 2}{2q \Re P_r B_{rx} + 4 k_b T_r B_{rx} / R_L} \tag{9}$$

where B_{rx} is the receiver bandwidth, q is the electrical charge $\approx 1.6 \times 10^{-19}$ c, k_b is the Boltzmann constant $\approx 1.38 \times 10^{-23}$ J/K, T_r is the receiver noise temperature, and R_L is the load resistance.

The photodiode detected signal is the amplified using an electrical amplifier with a gain of 40 dB. This amplified detected signal is now fed into a rectangular low pass filter (LPF) with cut-off frequency of 450 MHz along with RF-LFM signal to extract the required echo signal [53–56]. The beat signal after LPF is given as in Equation (10):

$$S_b(t) = A_c \Re P_r \beta \cos \left(2\pi f_c \tau - \frac{\pi B}{T_m} \tau^2 + 2\pi f_r t \right) \tag{10}$$

The filtered signal is the observed using the spectrum analyzer. The rest of the channels have a similar arrangement other than the operating wavelength. The parameters of the different components considered in the proposed photonic radar are given in Table 1.

Table 1. Photonic Radar Modeling Parameters.

Component	Parameter	Value
Continuous Wave laser	Wavelength	1550–1550.3 nm
	Channel Spacing	0.1 nm
	Linewidth	100 KHz
	Power	100 µW
Dual Port Mech-Zhender modulator (DP-MZM)	Extinction ratio	30 dB
	Switching bias voltage	4 V
	Switching RF voltage	4 V
	Bias voltage	0 V
Simulation window	Sweep time	10 µs
	No. of samples	8192
Photo detector (PIN)	Responsivity	1 A/W
	Dark current	1 nA
	Thermal and shot noise BW	410 MHz
	Absolute temp	290 k
	Load resistance	50 Ω

4. Results and Discussions

This section presents various observations and discusses the results obtained from direct detection-based, WDM-enabled photonic radar in a comprehensive manner. The proposed system used a total of 8192 samples for simulation purposes. Four different stationary targets are considered in the model with maximum distance of 150 m for target 1, 110 m for target 2, 60 m for target 3, and 15 m for target 4. The varying distances replicate the scenario in which a pedestrian, a cyclist, a car, as well as a large vehicle, such as a truck, are acting as targets on the road conditions. For the purpose of simulation, scintillations in free space are presumed to be ideal. Initially, the system is tested with bandwidth of 1 GHz under the clear weather conditions and similar results are obtained and compared at bandwidth of 4 GHz. Figure 3 illustrates the successful reception of reflected echoes from each of the four targets observed at the RF spectrum analyzer after filtering the unwanted signals at LPF with (a) at 1 GHz and (b) at 4 GHz bandwidth.
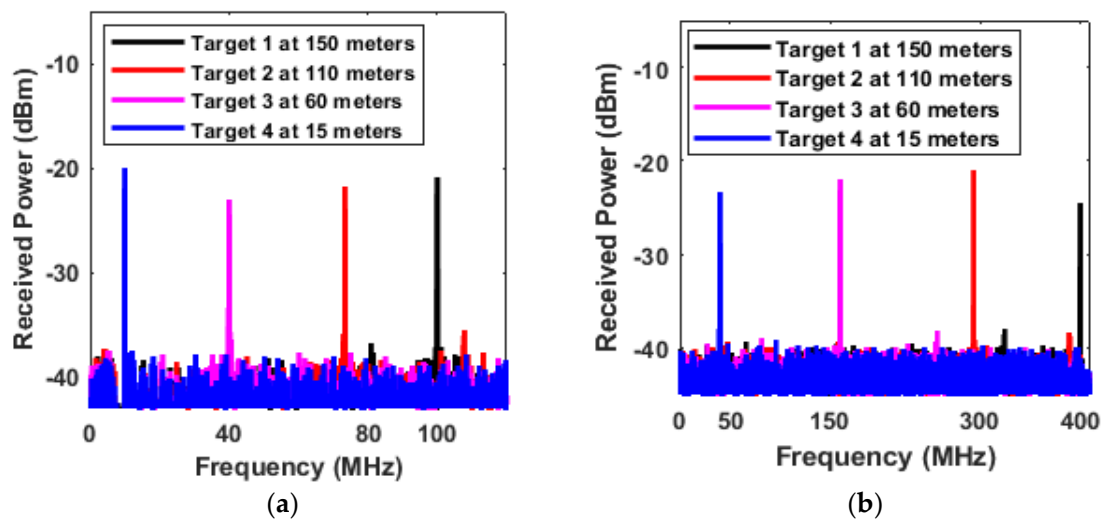

Figure 3. Power spectrum of de-chirped signal from multiple targets under clear atmospheric conditions (**a**) at 1 GHz and (**b**) at 4 GHz bandwidths.

Usually in radar operations, 90% of the transmitted power is either absorbed or scattered in the transmission, and only 10% of the power is considered reflected from the stationary targets. The clear peaks indicate range frequency for all the four targets at 1 GHz as well as for 4 GHz, as shown in Figure 3 depicting successful detection. Theoretically, the range frequency is calculated as given in Equation (1).

For 1 GHz bandwidth, the range frequency is theoretically calculated to be 100 MHz at 150 m, 73.33 MHz for 110 m, 40 MHz for 60 m, and 10 MHz for 15 m of target distance. The calculated theoretical values and similar detected range frequency peak is observed in Figure 3a. Likewise, when the bandwidth is changed to 4 GHz, the theoretically calculated range frequency is 400 MHz at 150 m, 293.33 MHz for 110 m, 160 MHz for 60 m, and 40 MHz for 15 m of target distance. Again, the calculated and observed peaks of the range frequency matches, as given in Figure 3b. This indicates successful detection of the multiple targets by the proposed WDM-enabled LFM-CW based photonic radar without any error.

The AV system relies on photonic radars for the effective performance of most of the conveniences and hence, should be able to detect effectively under the impact of atmospheric turbulences, particularly in low-visibility conditions to achieve the extended range detection. In the transportation sector, zero visibility is referred to as visibility of less than 50 m under adverse weather conditions that may leads to accidents [57]. Consequently, the performance of the proposed photonic radar is further studied under the impact of fog and rain. Fog is considered as a mixture of many aerosols in the air that results in degradation of overall system performance [58]. Another degrading factor in the

performance of the photonic radar is rain that affects the signal propagation, particularly at high frequencies, such as mm-band. The rain effect depends upon the rainfall rate (in mm/h) as well as the droplet size of the rain, as they both result in scattering or absorption. The theoretical value for calculation of attention due to rain (A_{rain})is given as [59]:

$$A_{rain} = k.R_o^\alpha \qquad (11)$$

where k and α are the power law factors that depend on variables, such as droplet size, frequency, and temperature, while R_o is the rate of rainfall in (mm/h).

The values of k and α can be computed via Marshall–Palmer distribution [60], and for the start frequency of 77 GHz, the values are calculated as 1.210 and 0.772. For this particular work we considered the values of attenuation in the modeling of the photonic radar system as specified in international visibility code [61] as 0 dB/km for clear weather, 2.5 dB/km for light rain (~2–3 mm/h), 12.5 dB/km for strong rain (~25 mm/h) and light fog, 25 dB/km for moderate fog, 50 dB/km for thick fog, and 70 dB/km for dense fog conditions. Another important aspect viz transmission losses, geometric losses, and additional losses are already considered, as explained in the system description. Figure 4 represents the successful reception of reflected echoes via the spectrum analyzer under the adverse effects of weather with attenuation of 50 dB/km.
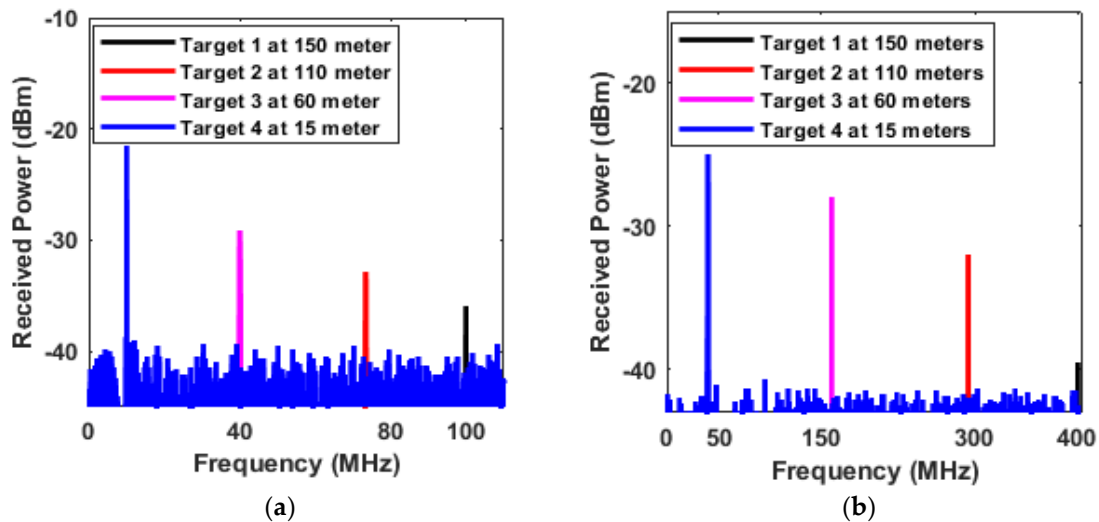

Figure 4. Power spectrum of de-chirped signal from multiple targets under adverse atmospheric conditions with attenuation of 50 dB/km (**a**) at 1 GHz and (**b**) at 4 GHz bandwidth.

The graph illustrates the impact of attenuation with higher bandwidth at mm-band attenuation severely affected power of echo signal at 150 m of range. Thus, it can be concluded that though the signal distortion is higher at the 4 GHz bandwidth with attenuation of 50 dB/km and an increasing target range from 15 m to 150 m; yet the proposed photonic radar successfully detected the target with minimum acceptable signal strength. The actual signal strength from the received echo signal is observed via the electrical analyzer before amplification under the varying values of attenuation, as defined above, while theoretical calculation of SNR is discussed above in Equation (9). Figure 5 depicts the corresponding observed values of received power and signal-to-noise ratio (SNR) with respect to range for bandwidth of 1 GHz up to 70 dB/km of attenuation.
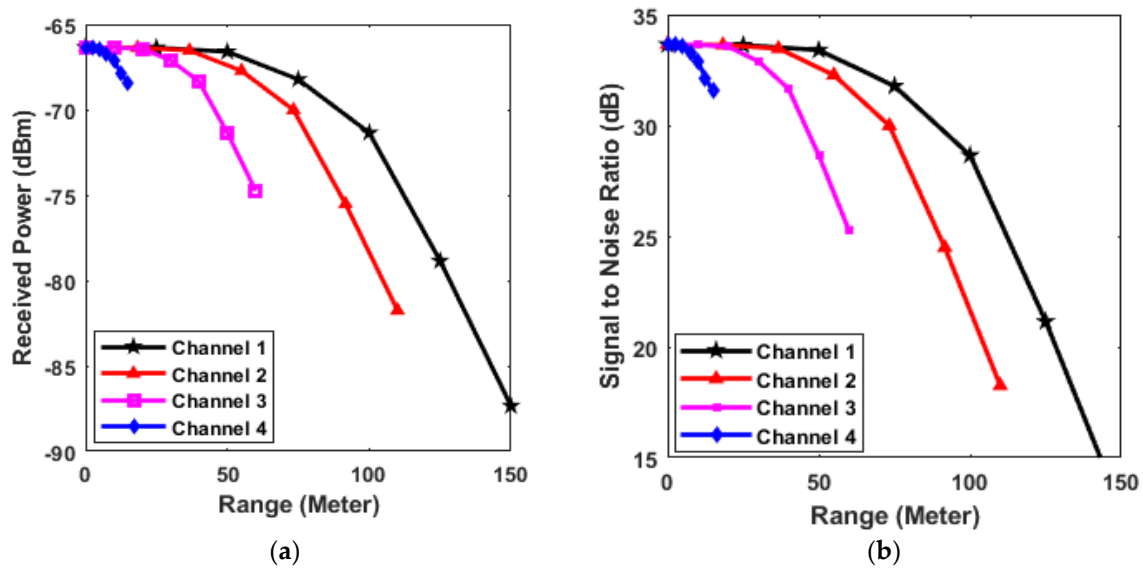
(**a**)   (**b**)

Figure 5. (**a**) Received power and (**b**) signal-to-noise ratio (SNR) with respect to range at 1 GHz bandwidth.

The effects of attenuation are detrimental with varying ranges, as shown in the graph in terms of the received power and signal-to-noise ratio. For instance, channel 4 has been placed at 15 m from the radar-equipped vehicle; hence, minimal effects of attenuation are observed in the channel 4 signal strength as well as the SNR, whereas it has a maximum effe3ct for the channel as it is placed at 150 m. At 0 dB/km, the received power is −66.34 dBm, while the reported SNR is 33.65 dB for all the channels, but as the attenuation increases, the received power and SNR degrades. For attenuation of 50 dB/km, the SNR and received power for channel 1 are 18.65 dB and −87.34 dBm, respectively, while for channel 4 they are 31.55 dB and −68.44 dBm, respectively. This depicts minimum effects upon channel 4 as compared to channel 1. Similarly, the system is tested under the attenuations of 2.5 dB/km, 12.5 dB/km, 25 dB/km, and 70 dB/km; the values of reported received power and SNR for each channel are shown in Table 2. From the table it is evident that the entire channels successfully received signal under the attenuation effects up to 50 dB/km with sufficient received power and minimum acceptable signal-to-noise ratio.

Table 2. Ghz Bandwidth.

	Power (dBm)				SNR (dB)			
Attenuation Level	**Ch 1 at 150 m**	**Ch 2 at 110 m**	**Ch 3 at 60 m**	**Ch 4 at 15 m**	**Ch 1 at 150 m**	**Ch 2 at 110 m**	**Ch 3 at 60 m**	**Ch 4 at 15 m**
Thick Fog (70 dB/km)	−87.34	−81.74	−74.74	−68.44	12.65	18.25	25.25	31.55
Heavy Fog (50 dB/km)	−81.34	−77.34	−72.34	−67.84	18.65	22.65	27.65	32.15
Moderate Fog (25 dB/km)	−73.84	−71.84	−69.34	−67.09	26.15	28.15	30.65	32.90
Strong Rain and Low Fog (12.5 dB/km)	−70.04	−69.09	−67.84	−66.72	29.90	30.90	32.15	33.27
Light Rain (2.5 dB/km)	−67.64	−66.89	−66.64	−66.42	32.90	33.10	33.35	33.57
Clear (0 dB/km)	−66.34	−66.34	−66.34	−66.34	33.65	33.65	33.65	33.65

Figure 6 depicts the corresponding observed values of the received power and signal-to-noise ratio with respect to range for bandwidth of 4 GHz and up to 50 dB/km of attenuations. As discussed in the case of 1 GHz, similar observations have been made in 4 GHz bandwidth. At 0 dB/km, the received power is reported as −67.59 dBm and SNR as 32.40 dB for all the channels. As the attenuation increases, the signal degradation

is reported highest at channel 1 being placed at 150 m and lowest at channel 4 placed at 15 m from the radar-equipped vehicles. At 50 dB/km attenuation, channel 1 reported received power as −82.58 dBm and measured SNR as 17.40 dB, while at channel 4 the received power is reported as −69.09 dBm and the SNR is measured as 30.90 dB. As the minimum acceptable SNR is kept at 15 dB, the results with 70 dB/km attenuation are not reported in the case of 4 GHz as the signal degrades below 10 dB SNR in that case. Table 3 contains the brief observed values of received power and SNR for all the channels at different conditions.
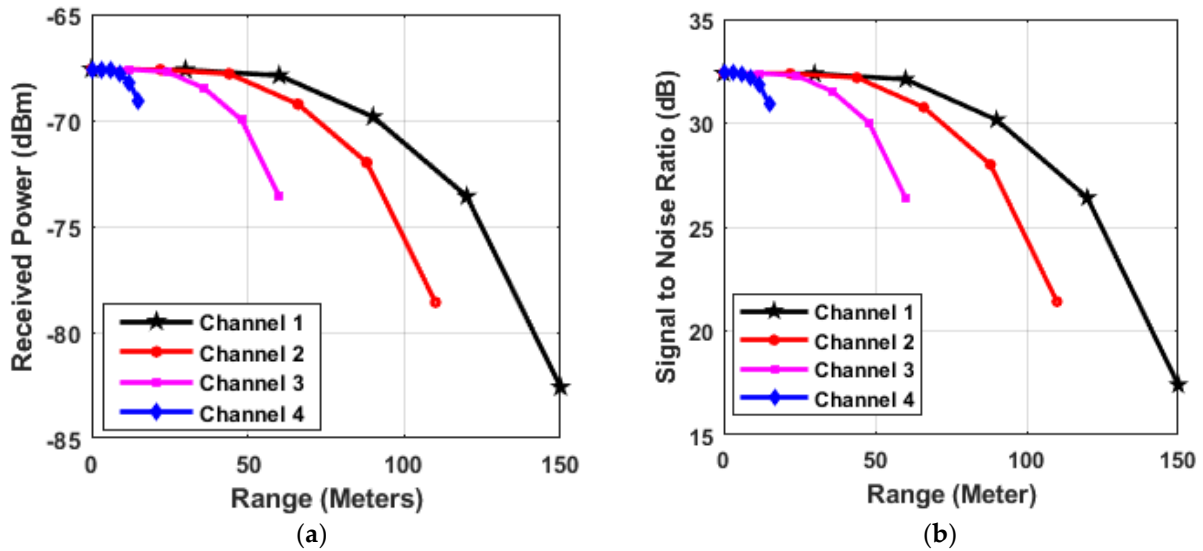

Figure 6. (**a**) Received power and (**b**) signal-to-noise ratio (SNR) with respect to range at 1 GHz bandwidth.

Table 3. Ghz Bandwidth.

Attenuation Level	Power (dBm)				SNR (dB)			
	Ch 1 at 150 m	Ch 2 at 110 m	Ch 3 at 60 m	Ch 4 at 15 m	Ch 1 at 150 m	Ch 2 at 110 m	Ch 3 at 60 m	Ch 4 at 15 m
Thick Fog (70 dB/km)	−82.58	−78.59	−73	−69.50	17.40	21.40	26.40	30.90
Heavy Fog (50 dB/km)	−75.89	−73.09	−70.59	−68.34	24.90	26.70	29.40	31.65
Moderate Fog (25 dB/km)	−71.34	−70.39	−69.09	−67.96	28.65	29.67	30.90	32.03
Strong Rain and Low Fog (12.5 dB/km)	−68.34	−68.14	−67.89	−67.66	31.65	31.85	32.10	32.33
Light Rain (2.5 dB/km)	−67.59	−67.59	−67.59	−67.59	32.40	32.40	32.40	32.40
Clear (0 dB/km)	−82.58	−78.59	−73	−69.50	17.40	21.40	26.40	30.90

From the above discussed Figures 5 and 6 as well as Tables 2 and 3, it can be concluded that attenuation effect increases with increase in bandwidth as well as range. Figure 7 shows the variations of SNR values with attenuation to further understand the variations in signal quality in varying atmospheric conditions. As discussed above and as depicted in Figure 7, the SNR in the case of 1 GHz bandwidth is better than in 4 GHz bandwidth.
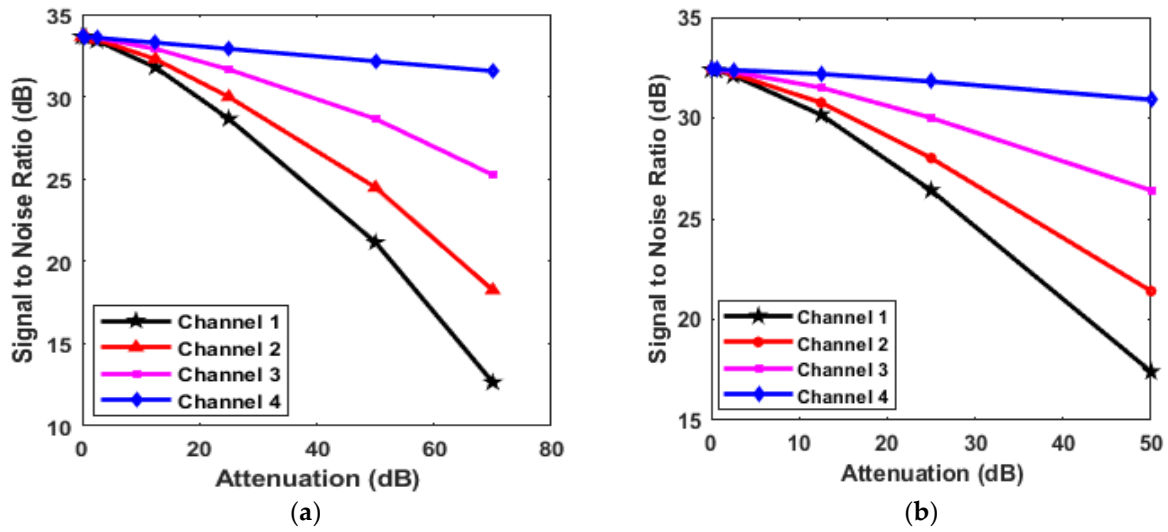
Figure 7. Signal-to-noise ratio versus attenuation (**a**) at 1 GHz bandwidth and (**b**) at 4 GHz bandwidth.

Another important parameter to realize autonomous vehicles is to distinguish between two closely located targets. Many times, autonomous vehicles find such a situation where two objects or vehicles are at the same distance and with very narrow spacing between them. Any mishap may occur if the AVs are not able to distinguish the difference between such close vehicles. This feature is known as range resolution and to the best of the author's knowledge, range resolution above 100 m of distance between the target vehicle and the radar-equipped vehicle is yet to be reported.

The range resolution, $L_{RES,}$ is defined as Equation (12) [21]:

$$L_{Res} = \frac{c}{2B} \tag{12}$$

where c is speed of light and B is bandwidth of the system. From Equation (12) it can be deducted that the range resolution depends upon the bandwidth of the frequency band utilized.

Theoretically, range resolution for 1 GHz of bandwidth is calculated as 15 cm, and for bandwidth of 4 GHz, range resolution is calculated as 3.75 cm using Equation (12). To test the proposed system for possible range resolution, we placed target 1 at 150 m and target 3 at 148 m. The simulation was performed with a displacement of 15 cm between targets 1 and 2 as well target 3 and 4 in the case of bandwidth 1 GHz, and displacement of 3.75 cm is given in the case of 4 GHz bandwidth between targets 1 and 2 as well target 3 and 4. Overlapping peaks were initially reported, and thus, the displacement is first increased to 30 cm and then to 50 cm in the case of 1 GHz bandwidth. Likewise, displacement shifted from 3.75 to initially 5 cm and then to 6.75 cm in the case of 4 GHz bandwidth. The clear peaks are observed at the displacement of 50 cm in the case of 1 GHz and 6.75 cm in the case of 4 GHz bandwidth between the targets, as shown in Figure 8.

The clear peaks of received echoes indicate the detection of all four vehicles at a distance of ~150 m, showing the realization of autonomous vehicles that can distinguish closely placed targets. The simulated results depict the system suffers an error of 35 cm in the case of 1 GHz bandwidth and 3 cm error in the case of 4 GHz bandwidth from the theoretically calculated values.
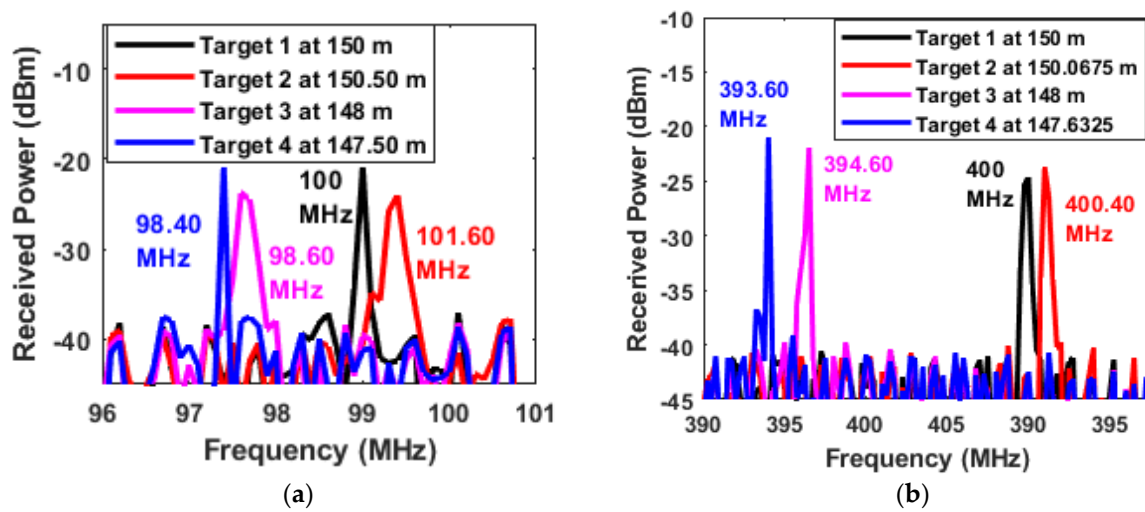
Figure 8. Power spectrum of de-chirped signal (**a**) separated by 50 cm at 1 GHz and (**b**) separated by 6.75 cm at 4 GHz.

Table 4 shows some of the previous works which indicate that the proposed photonic radar performs well in terms of target range and resolution, impact of turbulences, and the total number of targets identified concurrently.

Table 4. Performance Comparison with Recent Works.

Ref.	No. of Targets	Range	Operational Bandwidth	Range Resolution	Turbulences
[62]	1	15 m	24 and 77 GHz	Not Reported	Not Reported
[63]	1	11 m	40 GHz	Not Reported	Not Reported
[64]	1	1.72 m	8.5 to 12.5 GHz	5.9 cm	Not Reported
[65]	1	51 m	10 GHz	Not reported	Not reported
[66]	2	2 m	10 GHz	1.5 cm	Not reported
Our work	4	150 m	77 GHz	6.75 cm	Heavy Fog (70 dB/Km)

5. Conclusions

In this work, we designed a LFM-CW based photonic radar by incorporating WDM scheme for autonomous vehicle applications that can detect multiple stationary objects via the direct detection method. The key advantages of the proposed system are low-power requirement and compact size. Four targets placed at varying distances from the photonic radar-equipped vehicle were detected using 1 GHz and 4 GHz bandwidths in clear weather as well as under atmospheric turbulences. The results show improved power and SNR levels at the lower bandwidth of 1 GHz compared to the higher bandwidth of 4 GHz. The system is further tested for range resolution to identify the closely spaced targets at 150 m, and the reported results shows resolution of 50 cm in the case of 1 GHz of bandwidth and 6.75 cm in the case of 4 GHz of bandwidth. The reported results also show the significant improvement in range resolution as well as target detections compared to the previous works, as mentioned in Table 4. In the future, this work can be further extended to the moving targets and under complex traffic conditions.

References

1. World Health Organization. *Road Traffic Injuries*; World Health Organization: Geneva, Switzerland, 2021.
2. U.S. Department Transportation. *Automated Vehicles for Safety*; U.S Department Transportation: Washington, DC, USA, 2017.
3. Group, T. 7 Benefits of Autonomous Cars. 2017. Available online: https://www.thalesgroup.com/en/markets/digital-identity-and-security/iot/magazine/7-benefits-autonomous-cars (accessed on 30 August 2022).
4. Lee, H.; Yoon, J.; Jeong, Y.; Yi, K. Moving Object Detection and Tracking Based on Interaction of Static Obstacle Map and Geometric Model-Free Approachfor Urban Autonomous Driving. *IEEE Trans. Intell. Transp. Syst.* **2021**, *22*, 3275–3284. [CrossRef]
5. Skolnik, M.I. *Introduction to Radar Systems*; McGraw-Hill Education: New York, NY, USA, 1980.
6. Giese, T.; Klappstein, J.; Dickmann, J.; Wöhler, C. Road course estimation using deep learning on radar data. In Proceedings of the 2017 18th International Radar Symposium (IRS), Prague, Czech Republic, 28–30 June 2017; pp. 1–7.
7. Magnier, V.; Gruyer, D.; Godelle, J. Automotive LIDAR objects detection and classification algorithm using the belief theory. In Proceedings of the 2017 IEEE Intelligent Vehicles Symposium (IV), Los Angeles, CA, USA, 11–14 June 2017; pp. 746–751.
8. Cui, S.L.Z.; Ye, X.; Feng, J.; Yang, Y.; He, Z.; Cong, R.; Zhu, D.; Zhang, F.; Pan, S. Chip-based photonic radar for high-resolution imaging. *arXiv Preprint* **2019**, arXiv:1905.12802.
9. Li, S.; Cui, Z.; Ye, X.; Feng, J.; Yang, Y.; He, Z.; Cong, R.; Zhu, D.; Zhang, F.; Pan, S. Chip-Based Microwave-Photonic Radar for High-Resolution Imaging. *Laser Photonics Rev.* **2020**, *14*, 1900239. [CrossRef]
10. Bae, Y.; Shin, J.; Lee, S.G.; Kim, H. Field Experiment of Photonic Radar for Low-RCS Target Detection and High-Resolution Image Acquisition. *IEEE Access* **2021**, *9*, 63559–63566. [CrossRef]
11. Premebida, C.; Monteiro, G.; Nunes, U.; Peixoto, P. A lidar and vision-based approach for pedestrian and vehicle detection and tracking. In Proceedings of the 2007 IEEE Intelligent Transportation Systems Conference, Bellevue, WA, USA, 30 September–3 October 2007; pp. 1044–1049.
12. Sivaraman, S.; Trivedi, M.M. Looking at vehicles on the road: A survey of vision-based vehicle detection, tracking, and behavior analysis. *IEEE Trans. Intell. Transp. Syst.* **2013**, *14*, 1773–1795. [CrossRef]
13. Roriz, R.; Cabral, J.; Gomes, T. Automotive LiDAR Technology: A Survey. *IEEE Trans. Intell. Transp. Syst.* **2022**, *23*, 6282–6297. [CrossRef]
14. Shi, J.-W.; Guo, J.-I.; Kagami, M.; Suni, P.; Ziemann, O. Photonic technologies for autonomous cars: Feature introduction. *Opt. Express* **2019**, *27*, 7627–7628. [CrossRef]
15. Dudek, M.; Nasr, I.; Bozsik, G.; Hamouda, M.; Kissinger, D.; Fischer, G. System analysis of a phased-array radar applying adaptive beam-control for future automotive safety applications. *IEEE Trans. Veh. Technol.* **2014**, *64*, 34–47. [CrossRef]
16. Sharma, A.; Chaudhary, S.; Malhotra, J.; Parnianifard, A.; Wuttisittikulkij, L. Measurement of Target range and Doppler shift by incorporating PDM-enabled FMCW-based photonic radar. *Optik* **2022**, *262*, 169191. [CrossRef]
17. SHARMA, A.; Chaudhary, S.; Malhotra, J.; Saadi, M.; Otaibi, S.A.; Nebhen, J.; Wuttisittikulkij, L. A Cost-Effective Photonic Radar under Adverse Weather conditions for Autonomous Vehicles by incorporating Frequency Modulated Direct Detection Scheme. *Front. Phys.* **2021**, *467*. [CrossRef]
18. Chaudhary, S.; Wuttisittikulkij, L.; Saadi, M.; Sharma, A.; Al Otaibi, S.; Nebhen, J.; Rodriguez, D.Z.; Kumar, S.; Sharma, V.; Phanomchoeng, G. Coherent detection-based photonic radar for autonomous vehicles under diverse weather conditions. *PLoS ONE* **2021**, *16*, e0259438. [CrossRef] [PubMed]
19. Karlsson, C.J.; Olsson, F.Å. Linearization of the frequency sweep of a frequency-modulated continuous-wave semiconductor laser radar and the resulting ranging performance. *Appl. Opt.* **1999**, *38*, 3376–3386. [CrossRef]
20. Ghassemlooy, Z.; Popoola, W.; Rajbhandari, S. *Optical Wireless Communications: System and Channel Modelling With MATLAB®*; CRC Press: Boca Raton, FL, USA, 2019.
21. Zhang, F.; Guo, Q.; Pan, S. Photonics-based real-time ultra-high-range-resolution radar with broadband signal generation and processing. *Sci. Rep.* **2017**, *7*, 13848. [CrossRef] [PubMed]
22. Elghandour, A.H.; Ren, C.D. Modeling and comparative study of various detection techniques for FMCW LIDAR using optisystem. In Proceedings of the International Symposium on Photoelectronic Detection and Imaging 2013: Laser Sensing and Imaging and Applications, Beijing, China, 19 September 2013; p. 890529.
23. Sharma, A.; Malhotra, J. Simulative investigation of FMCW based optical photonic radar and its different configurations. *Opt. Quantum Electron.* **2022**, *54*, 233. [CrossRef]
24. Harris, M.; Young, R.I.; Köpp, F.; Dolfi, A.; Cariou, J.-P. Wake vortex detection and monitoring. *Aerosp. Sci. Technol.* **2002**, *6*, 325–331. [CrossRef]

25. Dolfi-Bouteyre, A.; Canat, G.; Valla, M.; Augere, B.; Besson, C.; Goular, D.; Lombard, L.; Cariou, J.-P.; Durecu, A.; Fleury, D. Pulsed 1.5-μ m LIDAR for Axial Aircraft Wake Vortex Detection Based on High-Brightness Large-Core Fiber Amplifier. *IEEE J. Sel. Top. Quantum Electron.* **2009**, *15*, 441–450. [CrossRef]
26. Kutila, M.; Pyykönen, P.; Ritter, W.; Sawade, O.; Schäufele, B. Automotive LIDAR sensor development scenarios for harsh weather conditions. In Proceedings of the 2016 IEEE 19th International Conference on Intelligent Transportation Systems (ITSC), Rio de Janeiro, Brazil, 1–4 November 2016; pp. 265–270.
27. Series, P. *Attenuation by Atmospheric Gases*; Springer: Dordrecht, The Netherlands, 2016.
28. Peynot, T.; Underwood, J.; Scheding, S. Towards reliable perception for unmanned ground vehicles in challenging conditions. In Proceedings of the 2009 IEEE/RSJ International Conference on Intelligent Robots and Systems, St. Louis, MO, USA, 10–15 October 2009; pp. 1170–1176.
29. Wojtanowski, J.; Zygmunt, M.; Kaszczuk, M.; Mierczyk, Z.; Muzal, M. Comparison of 905 nm and 1550 nm semiconductor laser rangefinders' performance deterioration due to adverse environmental conditions. *Opto-Electron. Rev.* **2014**, *22*, 183–190. [CrossRef]
30. Bijelic, M.; Gruber, T.; Ritter, W. A benchmark for lidar sensors in fog: Is detection breaking down? In Proceedings of the 2018 IEEE Intelligent Vehicles Symposium (IV), Changshu, China, 26–30 June 2018; pp. 760–767.
31. Rasshofer, R.H.; Spies, M.; Spies, H. Influences of weather phenomena on automotive laser radar systems. *Adv. Radio Sci.* **2011**, *9*, 49–60. [CrossRef]
32. Hasirlioglu, S.; Riener, A.; Huber, W.; Wintersberger, P. Effects of exhaust gases on laser scanner data quality at low ambient temperatures. In Proceedings of the 2017 IEEE Intelligent Vehicles Symposium (IV), Los Angeles, CA, USA, 11–14 June 2017; pp. 1708–1713.
33. Ramasubramanian, K.; Ramaiah, K. Moving from Legacy 24 GHz to State-of-the-Art 77-GHz Radar. *ATZelektronik Worldw.* **2018**, *13*, 46–49. [CrossRef]
34. Meena, D.; Francis, F.; Sarath, K.; Dipin, E.; Srinivas, T. Feasibility analysis of WDM links for radar applications. *Def. Technol.* **2015**, *11*, 76–84. [CrossRef]
35. Liu, X.; Wang, K. Research on high-resolution wide-swath SAR based on microwave photonics. In Proceedings of the 2016 CIE International Conference on Radar (RADAR), Guangzhou, China, 10–13 October 2016; pp. 1–3.
36. Li, R.; Li, W.; Ding, M.; Wen, Z.; Li, Y.; Zhou, L.; Yu, S.; Xing, T.; Gao, B.; Luan, Y. Demonstration of a microwave photonic synthetic aperture radar based on photonic-assisted signal generation and stretch processing. *Opt. Express* **2017**, *25*, 14334–14340. [CrossRef]
37. Meng, Z.; Li, J.; Yin, C.; Fan, Y.; Yin, F.; Zhou, Y.; Dai, Y.; Xu, K. Dual-band dechirping LFMCW radar receiver with high image rejection using microwave photonic I/Q mixer. *Opt. Express* **2017**, *25*, 22055–22065. [CrossRef] [PubMed]
38. Shibagaki, N. Experimental study of photonic based radar for FOD detection systems using 90 GHz-band. In *Air Traffic Management and Systems II*; Springer: Berlin, Germany, 2017; pp. 239–248.
39. Qian, N.; Zou, W.; Zhang, S.; Chen, J. Signal-to-noise ratio improvement of photonic time-stretch coherent radar enabling high-sensitivity ultrabroad W-band operation. *Opt. Lett.* **2018**, *43*, 5869–5872. [CrossRef]
40. Sharma, V.; Sergeyev, S. Range detection assessment of photonic radar under adverse weather perceptions. *Opt. Commun.* **2020**, *472*, 125891. [CrossRef]
41. Shakthi Murugan, K.H.; Sharma, A.; Malhotra, J. Performance analysis of 80 Gbps Ro-FSO system by incorporating hybrid WDM-MDM scheme. *Opt. Quantum Electron.* **2020**, *52*, 505. [CrossRef]
42. Chaudhary, S.; Chauhan, P.; Sharma, A. High Speed 4× 2.5 Gbps-5 GHz AMI-WDM-RoF Transmission System for WLANs. *J. Opt. Commun.* **2019**, *40*, 285–288. [CrossRef]
43. Zhou, Z.; Zhang, H.; Lin, C.; Sharma, A. Performance analysis of duobinary and CSRZ modulation based polarization interleaving for high-speed WDM-FSO transmission system. *J. Opt. Commun.* **2022**, *43*, 147–152. [CrossRef]
44. Chaudhary, S.; Sharma, A.; Chaudhary, N. 6 × 20 Gbps Hybrid WDM–PI Inter-satellite System under the Influence of Transmitting Pointing Errors. *J. Opt. Commun.* **2016**, *37*, 375–379. [CrossRef]
45. Chen, Y.; Weng, B.; Liu, J. A novel photonic-based MIMO radar architecture with all channels sharing a single transceiver. *IEEE Access* **2019**, *7*, 165093–165102. [CrossRef]
46. Dong, J.; Zhang, F.; Jiao, Z.; Sun, Q.; Li, W. Microwave photonic radar with a fiber-distributed antenna array for three-dimensional imaging. *Opt. Express* **2020**, *28*, 19113–19125. [CrossRef] [PubMed]
47. Yao, X.S.; Liu, X.; Hao, P. Scan-less 3D optical sensing/Lidar scheme enabled by wavelength division demultiplexing and position-to-angle conversion of a lens. *Opt. Express* **2020**, *28*, 35884–35897. [CrossRef] [PubMed]
48. Zhou, P.; Zhang, F.; Pan, S. Generation of linear frequency-modulated waveforms by a frequency-sweeping optoelectronic oscillator. *J. Lightwave Technol.* **2018**, *36*, 3927–3934. [CrossRef]
49. Coutinho, O.L.; Almeida, V.R.; Oliveira, J.E.B. Analysis of analog fiber optical links based on DSB+ C and SSB+ C modulation techniques. In Proceedings of the SBMO/IEEE MTT-S International Conference on Microwave and Optoelectronics, 2005, Brasilia, Brazil, 25 July 2005; pp. 439–443.
50. Hui, R.; O'Sullivan, M. *Fiber Optic Measurement Techniques*; Academic Press: San Diego, CA, USA, 2009.
51. Agrawal, G.P. *Fiber-Optic Communication Systems*; John Wiley & Sons: New York, NY, USA, 2012; Volume 222.
52. Keiser, G. *Optical Communications Essentials*; McGraw-Hill Education: Berkshire, UK, 2003.

53. Ricchiuti, A.L.; Hervás, J.; Barrera, D.; Sales, S.; Capmany, J. Microwave photonics filtering technique for interrogating a very-weak fiber Bragg grating cascade sensor. *IEEE Photonics J.* **2014**, *6*, 1–10. [CrossRef]
54. Marques, C.A.; Leal-Junior, A.G.; Min, R.; Domingues, M.; Leitão, C.; Antunes, P.; Ortega, B.; André, P. Advances on polymer optical fiber gratings using a KrF pulsed laser system operating at 248 nm. *Fibers* **2018**, *6*, 13. [CrossRef]
55. Cheng, B.; Song, Y.; Hua, L.; Xiao, H. Fabrication and characterization of femtosecond laser induced microwave frequency photonic fiber grating. *J. Lightwave Technol.* **2020**, *38*, 5286–5292. [CrossRef] [PubMed]
56. Liang, H.; Ying, K.; Wang, D.; Pi, H.; Li, X.; Wang, Z.; Wei, F.; Cai, H. All-fiber narrow-bandwidth rectangular Optical filter with reconfigurable bandwidth and tunable center wavelength. *Opt. Express* **2021**, *29*, 11739–11749. [CrossRef]
57. Miclea, R.-C.; Dughir, C.; Alexa, F.; Sandru, F.; Silea, I. Laser and LIDAR in A system for visibility distance estimation in fog conditions. *Sensors* **2020**, *20*, 6322. [CrossRef]
58. Al Naboulsi, M.C.; Sizun, H.; de Fornel, F. Fog attenuation prediction for optical and infrared waves. *Opt. Eng.* **2004**, *43*, 319–329. [CrossRef]
59. Rashidi, F.; He, J.; Chen, L. Spectrum slicing WDM for FSO communication systems under the heavy rain weather. *Opt. Commun.* **2017**, *387*, 296–302. [CrossRef]
60. Olsen, R.; Rogers, D.; Hodge, D. The aRbrelation in the calculation of rain attenuation. *IEEE Trans. Antennas Propag.* **1978**, *26*, 318–329. [CrossRef]
61. Awan, M.S.; Marzuki; Leitgeb, E.; Hillbrand, B.; Nadeem, F.; Khan, M.S. Cloud attenuations for free-space optical links. In Proceedings of the 2009 International Workshop on Satellite and Space Communications, Siena, Italy, 9–11 September 2009; pp. 274–278.
62. Serafino, G.; Amato, F.; Maresca, S.; Lembo, L.; Ghelfi, P.; Bogoni, A. Photonic approach for on-board and ground radars in automotive applications. *IET Radar Sonar Navig.* **2018**, *12*, 1179–1186. [CrossRef]
63. Wang, Y.; Hou, X.; Li, T.; He, Z.; Wang, D.; Yang, F.; Zhou, T.; Rong, L. Simultaneous detection of the distance and direction for a noncooperative target based on the microwave photonic radar. *Opt. Express* **2021**, *29*, 31561–31573. [CrossRef] [PubMed]
64. Liang, D.; Jiang, L.; Chen, Y. Multi-Functional Microwave Photonic Radar System for Simultaneous Distance and Velocity Measurement and High-Resolution Microwave Imaging. *J. Lightwave Technol.* **2021**, *39*, 6470–6478. [CrossRef]
65. Ding, Y.; Guo, S.; Wu, H.; Wang, D.; Li, J.; Yang, Y.; Cui, F.; Dong, W. Dual-Chirp Photonics-Based Radar for Distance and Velocity Measurement Based on Compressive Sensing. *IEEE Photonics J.* **2022**, *14*, 5541807. [CrossRef]
66. Bai, W.; Li, P.; Zou, X.; Zhou, Z.; Pan, W.; Yan, L.; Luo, B.; Fang, X.; Jiang, L.; Chen, L. Millimeter-wave joint radar and communication system based on photonic frequency-multiplying constant envelope LFM-OFDM. *Opt. Express* **2022**, *30*, 26407–26425. [CrossRef]